16th World Conference on Earthquake, 16WCEE 2017

Santiago Chile, January 9th to 13th 2017

Paper N° 2573

Registration Code: S-T1461697787

INCREASED SUBSTRUCTURE FLEXIBILITY ON COLUMN-TOP ISOLATION SYSTEMS

A. P. Crowder[(1)], T. C. Becker[(2)]

[(1)] *M.A.Sc. Candidate, McMaster University, crowdeap@mcmaster.ca*
[(2)] *Assistant Professor, McMaster University, tbecker@mcmaster.ca*

Abstract

As seismic isolation continues to gain popularity for its ability to significantly reduce earthquake damage, retrofit applications are still limited due to significant construction expenses. Foundation work and excavation of a seismic gap, as well as installation of an additional rigid diaphragm lead to high project costs which often limit isolation retrofit to historical buildings. To mitigate these expenses, some designers have begun installing the isolation layer on the tops of the first level columns without the use of an additional rigid diaphragm. This type of installation also negates the need for excavation; however, designers typically design practically rigid support columns in an effort to limit any flexibility below the isolation plane. While this is practical for new construction, this may not be feasible for a retrofit application. This study considers the behavior of a column-top isolation system when subjected to varying substructure flexibilities. Large flexibility leads to end rotations in the isolation bearings during ground motions. To investigate this behavior, experimental cyclic testing of a column-bearing subsystem was done at McMaster University. The results are investigated and compared against a bearing model which accounts for changes in lateral stiffness and buckling behavior under both translational and rotational degrees of freedom, which was implemented in OpenSees. Experimental results show that flexible substructures can significantly reduce the lateral stiffness of elastomeric bearings and the end conditions must be accounted for to reasonably estimate the isolation period.

Keywords: Isolation; Retrofit; Elastomeric; Flexibility; Rotation

1. Introduction

Seismic isolation continues to gain popularity worldwide as a technique to effectively reduce the damages caused by earthquakes. Traditional installations of isolation systems are composed of a flexible layer located between the ground and the superstructure, bound by rigid diaphragms above and below. The rigid diaphragms ensure optimal performance of the bearings by distributing shear forces and maintaining parallel end plates of the isolators. During seismic events, the flexible layer decouples the structure from the ground and concentrates displacements to the isolation bearings, resulting in reduced interstory drifts and floor accelerations in the superstructure. To accommodate the lateral displacement in the layer, a seismic gap is required around the perimeter of the structure.

For the seismic rehabilitation of existing structures, isolation has been shown to significantly improve the response of at-risk structures [1]. Numerous isolation retrofit projects have been conducted around the world, but the process is often associated with large project costs [2]. For new construction, the installation of an isolation system typically adds 5% to project costs; however, retrofit applications tend to run significant costs, with the isolators themselves only accounting for a small percentage of the total expenses. The major costs associated with isolation retrofit come from excavation beneath the structure and of the seismic gap, installation of an additional rigid diaphragm, and foundation work that may be necessary. As a result of the high cost of isolation retrofit, applications are generally limited to structures with historical significance or that require immediate occupancy following seismic events. To reduce the cost and extend isolation retrofit to a more general class of structures, bearings may be placed on the tops of columns [1] as shown in Fig. 1, referred to here as column-top isolation. This type of installation eliminates the need for the construction of an additional rigid diaphragm, excavation beneath the building and of the seismic gap, and may avoid improvements to existing foundations.

New construction can also benefit from cost savings using column-top isolation, and a handful of projects have adopted the method. Examples include the Main Building of the Institute of Technology by the Shimizu Corporation in Japan [5]; the Justice and Emergency Services Precinct in New Zealand [6]; and an extension to the Tipping Structural Engineers office in the United States [7]. In each of these applications, designers have used large, stiff supporting columns to provide rigid boundary conditions for the isolation bearing, similar to using a rigid diaphragm. While this is sound practice, this may not always be economical or feasible, especially for retrofit applications when supporting columns may need significant work to provide rigid boundary conditions for isolators. Thus, supporting columns in the substructure may be flexible and allow bearing end plates rotation during displacements. While most models for isolation bearings assume end plates remain parallel, the assumption is no longer valid when substructure flexibility is present, and the behavior of the bearings can change. Flexible end conditions for friction pendulum bearings have been investigated [6,7]; however, studies on elastomeric bearings have mostly been limited to fixed amounts of rotation [8,9].

To investigate the effects of flexible end conditions on elastomeric bearings in column-top isolation systems, experimental testing of multiple column-bearing subassemblies were conducted at McMaster University. Four subassemblies with increasing column flexibility were tested under quasi-static cyclic motions to study the column-bearing interaction and the behavior of elastomeric bearings with varying boundary condition flexibility. For future studies, an analytical model was derived to represent the behavior of the bearings, and was adapted into a new element for use with OpenSees software [10]. Numerical simulations of

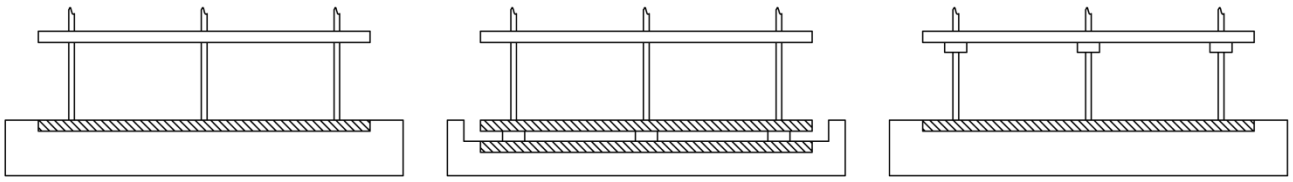

Fig. 1 – Comparison of pre-retrofit structure (left), traditional isolation (middle), and column-top isolation (right)

the experimental setup were compared to assess the validity of the model. The results of the study are applicable in a range of scenarios where elastomeric bearings may be susceptible to flexible end conditions, such as isolation of bridges, tall building isolation which experiences rocking along with translation, and bearing connections to flexible diaphragms.

2. Analytical Model

Modelling of elastomeric bearings often employs Haringx theory [11], which was introduced to study the buckling of short rubber rods under compression. The theory describes the deformations along the height of the rubber by independent variables for lateral displacement and rotation, and accounts for the large shear deformations expected with short rubber specimens. Later, Gent [12] extended the theory to study the buckling behavior of stacked rubber blocks separated by steel plates. The collection of rubber and steel was simplified to a homogeneous material, and the expected behavior compared well with experimental results. Imbimbo and Kelly [13] studied the effects of end plate flexibility on the buckling load of elastomeric bearings by modifying the boundary conditions used in the solution to Haringx theory, and determined the buckling load of a fixed-free configuration can be half of that of an equivalent fixed-fixed bearing. The lateral behavior of an elastomeric bearing with constant rotations present at the top, bottom, or both end plates was investigated by Karbakhsh Ravari et al. [8], and found that small rotations can significantly increase or decrease the lateral stiffness depending on the direction or rotation relative to the direction of translation. Chang [14] used the theory to impose various boundary conditions and derived a stiffness matrix for an individual rubber layer with translational and rotation degrees of freedom. Rigid offsets were used to account for steel shims, and an elastomeric bearing was constructed from many stiffness matrices for each rubber-shim layer, resulting in a very large stiffness matrix for the bearing. Constant loads were applied to fixed-fixed and fixed-free models and it was found that a free end can significantly reduce the lateral stiffness.

The model derived for this study generally followed the methodology proposed by Chang [14], and is presented in full in [14]. Instead of a stiffness matrix for each layer, a single four degree of freedom stiffness matrix was derived to model the entire bearing. The model assumes a homogeneous material, and to account for the steel shims a factor of h/t_r is applied to the shear and flexural stiffness terms, where h is the total height of the bearing, and t_r is the total thickness of all rubber layers [2]. The remaining necessary parameters for the model are: the axial load on the bearing, P; the modified shear stiffness, GA_a; and the modified flexural stiffness, EI_s. The resulting stiffness matrix for the bearing, corresponding to the degrees of freedom shown in Fig. 2, was determined as

$$\begin{bmatrix} V_1 \\ M_1 \\ V_2 \\ M_2 \end{bmatrix} = \frac{P}{2\lambda - \alpha\beta h} \begin{bmatrix} \alpha\beta & -\lambda & -\alpha\beta & -\lambda \\ -\lambda & \frac{1}{\alpha\beta} - \frac{h}{\tan(\alpha h)} & \lambda & -\frac{1}{\alpha\beta} + \frac{h}{\sin(\alpha h)} \\ -\alpha\beta & \lambda & \alpha\beta & \lambda \\ -\lambda & -\frac{1}{\alpha\beta} + \frac{h}{\sin(\alpha h)} & \lambda & \frac{1}{\alpha\beta} - \frac{h}{\tan(\alpha h)} \end{bmatrix} \begin{bmatrix} u_1 \\ \phi_1 \\ u_2 \\ \phi_2 \end{bmatrix} \quad (1)$$

where α, β, and λ are defined as

$$\alpha^2 = \frac{P(P+GA_s)}{EI_s GA_s} \qquad \beta = \frac{GA_s}{P(P+GA_s)} \qquad \lambda = \tan\left(\frac{\alpha h}{2}\right)$$

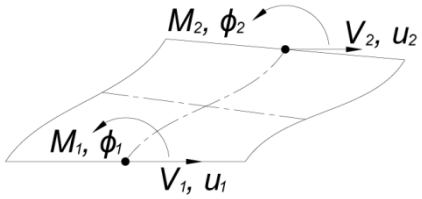

Fig. 2 – Degrees of freedom for the bearing model

For a circular bearing with radius *r*, rubber layer thickness *t*, shear modulus *G*, and bulk modulus *K*, the modified shear and flexural stiffness terms are

$$GA_s = \pi G r^2 \left(\frac{h}{t_r} \right) \tag{2}$$

$$EI_s = \frac{\pi G r^6}{8t^2} \left(1 - \frac{3Gr^2}{4Kt^2} \right) \left(\frac{h}{t_r} \right) \tag{3}$$

where the flexural stiffness is based on a pressure solution presented by Kelly and Konstantinidis [16], accounting for compressibility of the rubber. The model was adapted into a new element for OpenSees [10], where numerical simulations of the experimental setup were performed.

3. Experimental Setup

An experimental setup was designed and constructed to test four column-bearing subassemblies at ¼ scale. To simplify the setup, pictured in Fig. 3, the isolation bearing was installed at the bottom of the column rather than at the top. Two vertical actuators were used to apply a constant axial load to the subassembly through a loading beam, which was kept horizontal to act as a rigid foundation. A horizontal actuator provided the displacement control of a uniaxial table constructed beneath the subassembly. Load cells measured axial load, shear, and moment the bottom of the bearing. Displacements were measured at the base of the subassembly as well as at the column-bearing interface. An inclinometer captured the rotation of the column-bearing interface, and strain gauges were installed along the height of the column to determine bending moments.

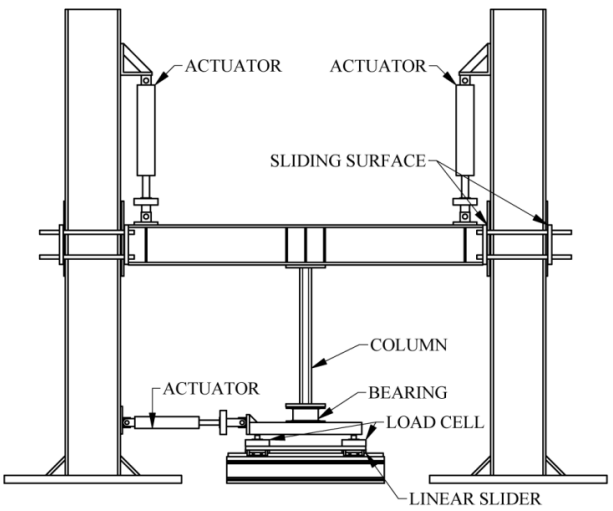

(a)

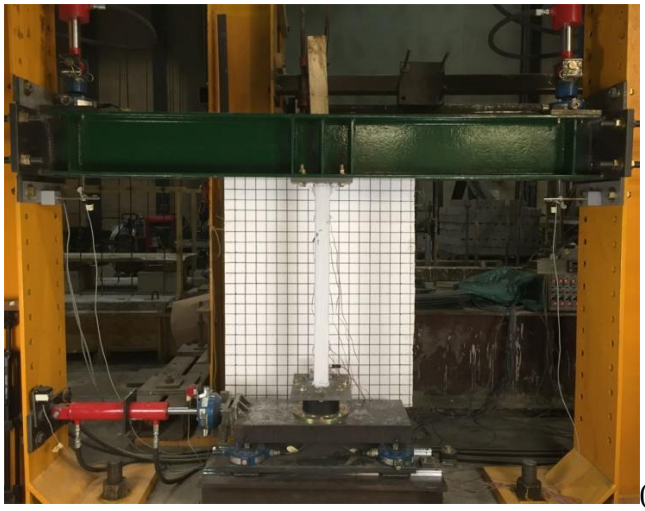

(b)

Fig. 3 – (a) Schematic of the experimental setup; (b) Constructed setup with HSS64x64x4.8 column installed

Table 1 – Column specimens in order of decreasing stiffness

Column Size	I (10^6 mm^4)	SR (%)
HSS127x127x8.0	7.73	2.9
HSS102x102x8.0	3.72	6.1
HSS76x76x4.8	1.00	22.7
HSS64x64x4.8	0.55	41.0

A typical circular elastomeric isolation bearing, manufactured to scale, was used for all subassemblies. The relevant properties of the bearing were: 160 mm diameter, 20 layers of rubber 1.98 mm thick, 19 steel shims 1 mm thickness, shear modulus of 0.4 MPa, and bulk modulus of 1300 MPa. The shape factor of the bearing was 20.2. All columns were steel square HSS sections with a length of 875 mm, and various section sizes were selected to provide a range of flexibilities and yielding behavior. The selected columns sections are listed in Table 1. The stiffest column was chosen to provide a near-rigid end condition for the bearing with small rotations and no yielding behavior. The most flexible column was selected to undergo large rotations at the column-bearing interface and yielding, undesirable behavior for column-top isolation systems. Included in Table 1 is a stiffness ratio, defined as the lateral stiffness ratio of the bearing over the column and given as

$$SR = \frac{k_b}{k_c} = \frac{GA/t_r}{3(EI)_c / L^3} \tag{4}$$

where $(EI)_c$ is the flexural stiffness of the column, and L is the length of the column. The ratio describes the column flexibility in comparison to the bearing, with a ratio of zero indicating a rigid column. It should be noted that the column lateral stiffness is determined as a fixed-free column, which will be discussed later.

Testing of all four subassemblies and of the bearing only was performed under quasi-static cyclic testing at a constant velocity of 1 mm/s, while an axial load was maintained to provide 6 MPa of pressure on the bearing. Each test followed the same displacement history with multiple loops at +/- 10 mm, +/- 20 mm, +/- 40 mm, +/- 60 mm, +/- 80 mm, and +/- 100 mm. However, testing of the HSS64x64x4.8 subassembly was stopped at the end of the +/- 80 mm cycles due to a negative tangential stiffness. The experimental setup was modelled in OpenSees [12] using the bearing model discussed previously. The columns were modelled with non-linear beam column elements with fiber sections. A Menegotto-Pinto model with strain hardening was used to describe the yielding behavior of the steel columns. The simulations underwent the same displacement history used in the experimental testing while a constant axial load was applied to the column-bearing subassembly.

4. Results and Discussion

Comparison of the shear-displacement hystereses loops for the HSS127x127x8.0 and the HSS76x76x4.8 subassemblies is shown in Fig. 4, and indicate a lower stiffness for the more flexible column as expected. However, the lower stiffness is not solely due to a more flexible column. Considering the hystereses of the bearing only (Fig. 4 right), determined by subtracting out the column displacements, the lateral stiffness of the bearing is also seen to reduce. This is a direct result of increasing the end condition flexibility for the isolation bearing. In addition, comparison of the bearing hystereses shows the bearing undergoes less displacement in the more flexible subassembly, due to the higher displacements in the column.

The secant stiffness of the bearing at the end of each displacement cycle is plotted in Fig. 5 for each column to show the stiffness degradation with increasing shear strain. Initially, the bearing was tested without a column installed to determine the baseline behavior, and the stiffness compares well with the design stiffness assumed at a shear strain of 100%. As more flexible end conditions were allowed for the bearing, the decrease in stiffness was magnified. In the case of the most flexible column, the lateral stiffness of the bearing decreased to

as low as 58% of the design stiffness. Thus, flexible end conditions can significantly alter the lateral stiffness of a bearing and must be accounted for to provide accurate estimates of the isolation period and peak displacement.

The shear- and moment-displacement hystereses for the bearing without a column connected are shown in Fig. 6 with comparisons to the numerical results. Under this test, the bearing end plates remained parallel, leading to behavior traditionally expected from elastomeric bearings. The derived model effectively predicted the secant stiffness of the bearing, along with the bending moment that develops at the column-bearing interface with increasing displacement. In comparison to this test, the response of the bearing with the HSS127x127x8.0 column is displayed in Fig. 7. With the installation of the stiffest column, the bearing had a near-rigid end condition, resulting in a small peak rotation of 0.6˚ at the column-bearing interface. Displacement demands were largely concentrated in the bearing due to the high stiffness of the column, and the column remained elastic. The

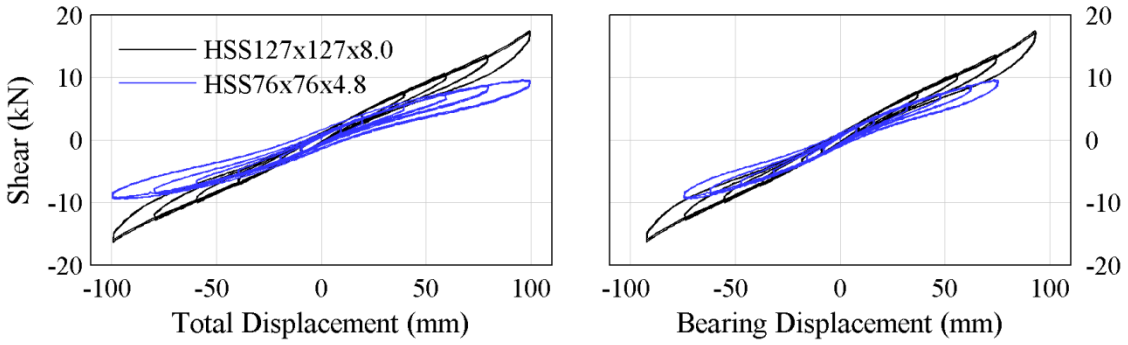

Fig. 4 – Experimental hysteresis for the subassembly (left), and bearing only (right)

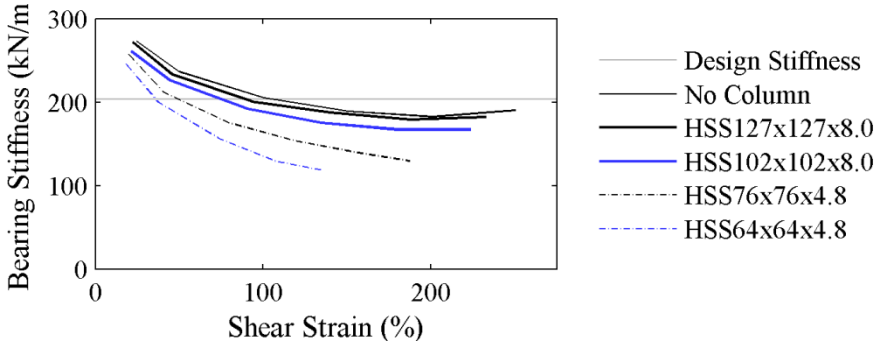

Fig. 5 – Bearing lateral stiffness degradation with increasing shear strain

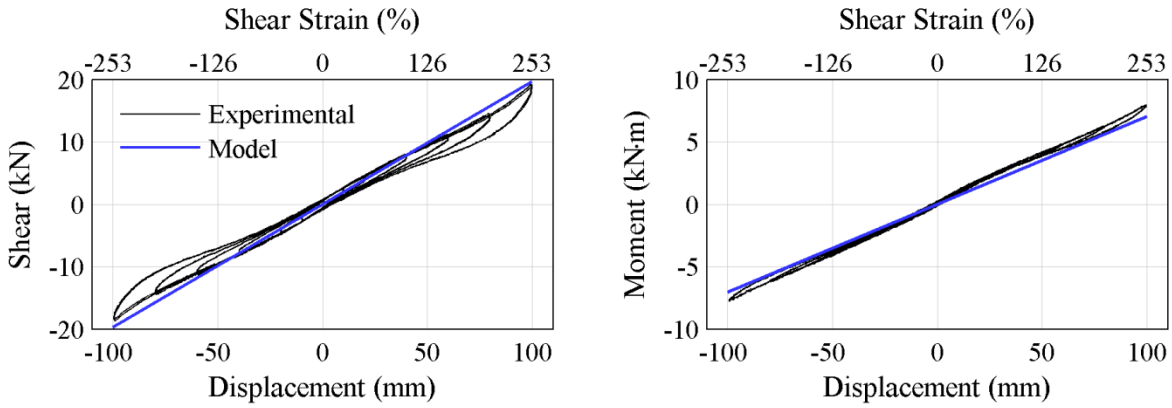

Fig.6 – Comparison of experimental and theoretical response of the bearing only

model compared well with the test results with the exception of the rotation at the column-bearing interface, which was underestimated by the model.

In contrast to the stiffest subassembly, the response of the bearing with the most flexible column is shown in Fig. 8. Testing of this subassembly resulted in large displacements in the column and yielding at the column end farthest from the bearing. Large rotations of 2.5˚ were recorded at the column-bearing interface resulting in a significantly lower lateral stiffness of the bearing. The model proved accurate for small deformations, however, at larger deformations nonlinear behavior was observed in the bearing response causing theoretical results to diverge from experimental. An interesting comparison between Fig. 7 and Fig. 8 is the change of sign for the

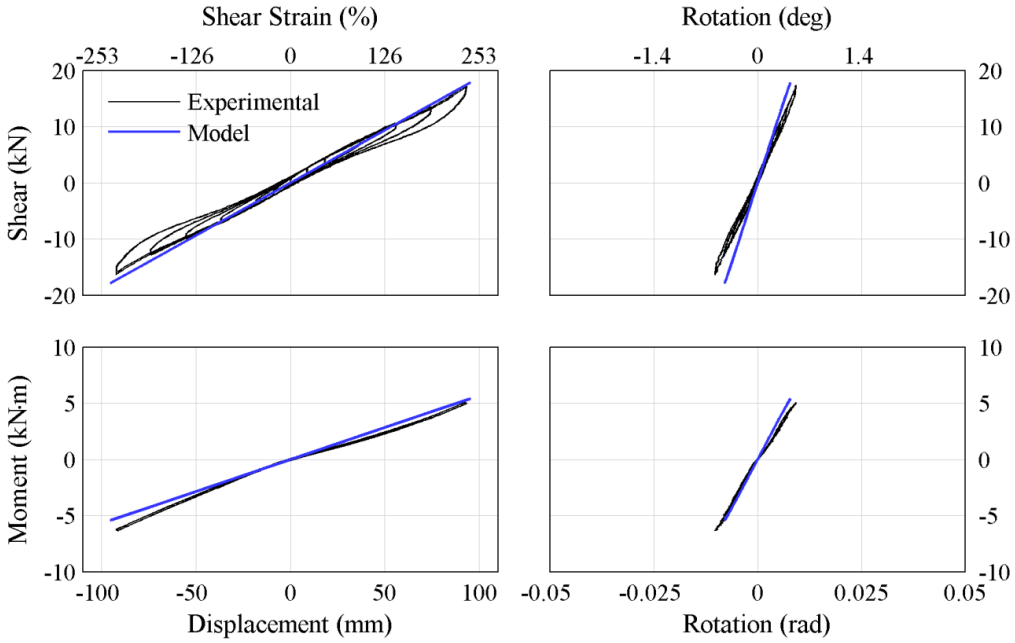

Fig. 7 – Comparison of experimental and theoretical response of the HSS127x127x8.0 subassembly

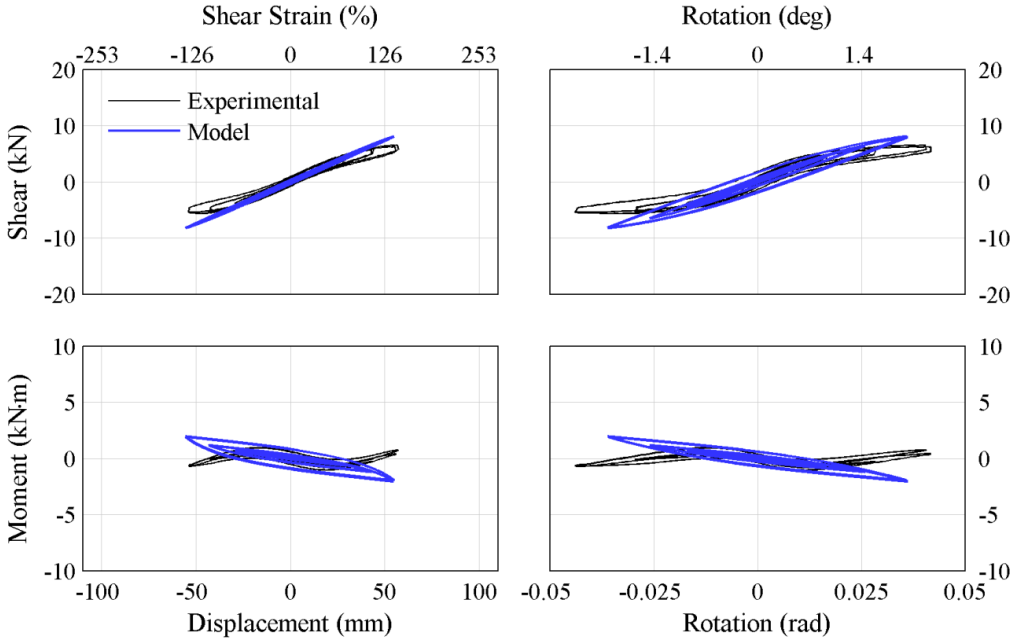

Fig. 8 – Comparison of experimental and theoretical response of the HSS64x64x4.8 subassembly

moment relationships. This was observed in the experimental bending moment diagrams in Fig. 9, determined at a displacement in the linear range of the bearing. The diagrams show the point of inflection moving from the midheight of the bearing and into the column with more flexible subassemblies. In the case of a rigid column, the inflection point should theoretically be located at the midheight of the bearing, affirming the HSS127x127x8.0 column provided a near-rigid condition. With the HSS127x127x8.0 and HSS102x102x8.0 columns, the bearing is shown to have a positive moment relationship at the top of the bearing, and undergoes double curvature. For the HSS76x76x4.8 and HSS64x64x4.8 columns, the bending moment at the top of the bearing changes signs, and the bearing undergoes single curvature. It is also noted from the bending moment diagrams that the moment at the column-bearing interface is small in comparison to the moment at the base of the column. For moderately flexible columns, the bending moment diagram is similar to that of a fixed-free structure, and thus supporting columns can be treated as fixed-free when determining the column lateral behavior.

The nonlinear behavior observed in the bearing moment in the HSS64x64x4.8 subassembly was also observed in the HSS76x76x4.8 and HSS102x102x8.0 subassemblies; however, the nonlinearity was less pronounced with stiffer columns. Using the results from the bearing without a column in Fig. 6, the moment displacement relationship was found to be linear, and if this is assumed to remain true when rotations exist, the nonlinear response must be a result of the moment-rotation relationship. This relationship can be isolated by considering the total moment as components of moment caused by displacement and rotation, and is given as

$$M = \begin{bmatrix} k_{\Delta} & k_{\theta} \end{bmatrix} \begin{bmatrix} \Delta \\ \theta \end{bmatrix} \tag{5}$$

where k_{Δ} and k_{θ} are the stiffness terms for the displacement of the bearing, Δ, and the rotation of the column-bearing interface, θ, respectively. Obtaining k_{Δ} as the secant stiffness from the moment-displacement relationship in Fig. 6, when rotations were zero, the component of moment caused by rotation can be isolated by

$$M - k_{\Delta}\Delta = k_{\theta}\theta \tag{6}$$

Using the measured values for moment, displacement, and rotation, the component of moment caused by rotation can be determined and is shown in Fig. 10 for each subassembly. The results of this process show a negative relationship, which was indicated by the decrease in moment as rotations at the column-bearing interface increased, shown in the trends of the bending moment diagrams at the column-bearing interface in Fig. 9. Included in the moment-rotation relationships in Fig. 10 is the theoretical stiffness derived in the model. The theoretical stiffness compares well to experimental results at small rotations; however, at rotations of 0.5˚ the moment-rotation relationship undergoes repeatable softening behavior. The linear bearing model is unable to account for this softening characteristic, reducing the range of accuracy for the model to particular values of end

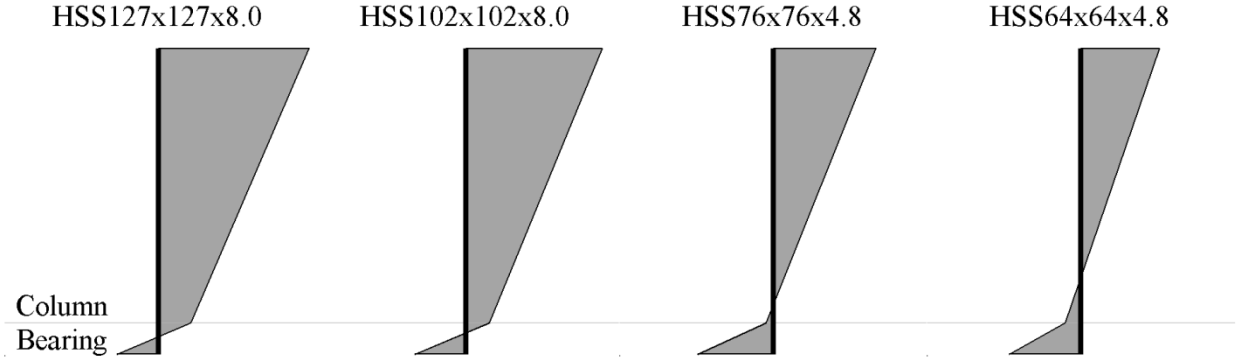

Fig. 9 – Experimental bending moment diagrams

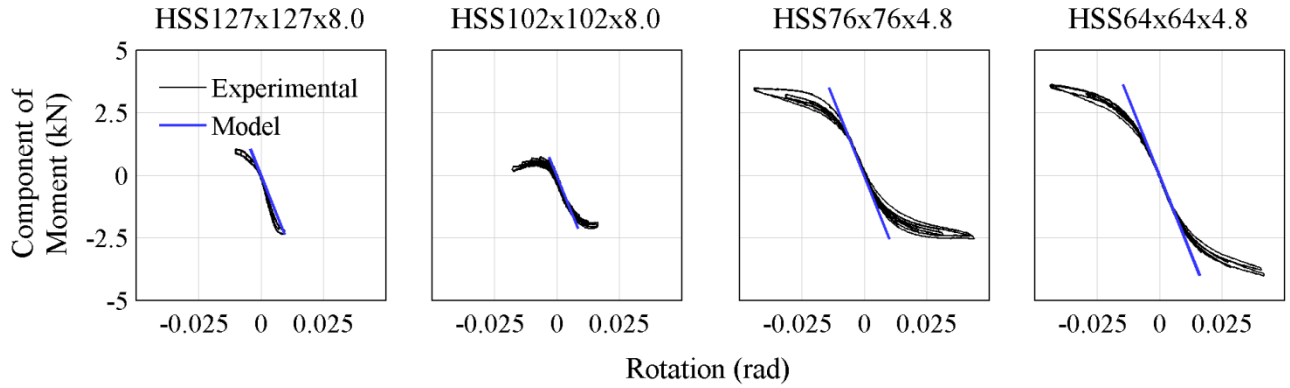

Fig. 10 – Component of moment at the bearing end plate due to rotation

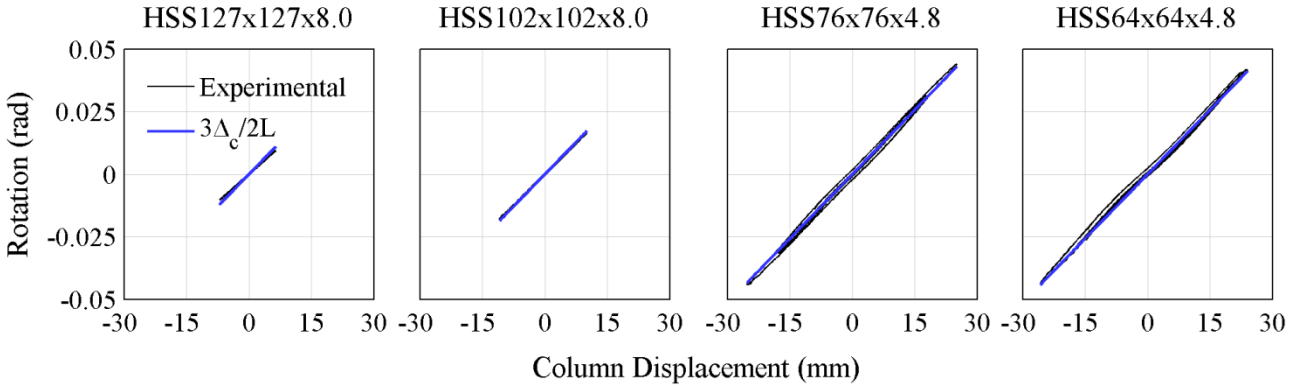

Fig. 11 – Relationship between column displacement and column-bearing interface rotation

plate rotations. This study found the softening to occur at a rotation of 0.5˚ for the elastomeric bearing used in this investigation; however, future investigations are necessary to determine at which value this behavior occurs for other bearing designs.

To estimate the amount of rotation at the column-bearing interface, a relationship was found with the column displacement. As a result of the high rotational stiffness, the column was found to govern the interface rotations. Using Euler-Bernoulli beam theory and assuming a fixed-free structure, the interface rotation, θ, can be determined using

$$\theta = \frac{3\Delta_c}{2L} \tag{7}$$

where Δ_c is the column displacement and L is the length of the column. Comparisons of the relationship with experimental results are shown in Fig. 11. The expression accurately predicts the column-bearing interface rotation for each column tested with the exception of the HSS127x127x8.0 column. The stiffest column had non-negligible shear deformations, which can increase displacements without causing rotations. This behavior, not accounted for in Eq. (7), results in the rotations at the column-bearing interface to be slightly overestimated by the expression.

The effect of the stiffness ratio on the peak column displacement ratio and peak column base moment was investigated and shown in Fig. 12. The column displacement ratio, a percentage of the column displacement from the total subassembly displacement, and base moment, the maximum occurring moment in the column, shows good agreement between theoretical and experimental results. The model slightly underestimated the column displacement as a result of not capturing the increase in total moment due to the nonlinear effects, which

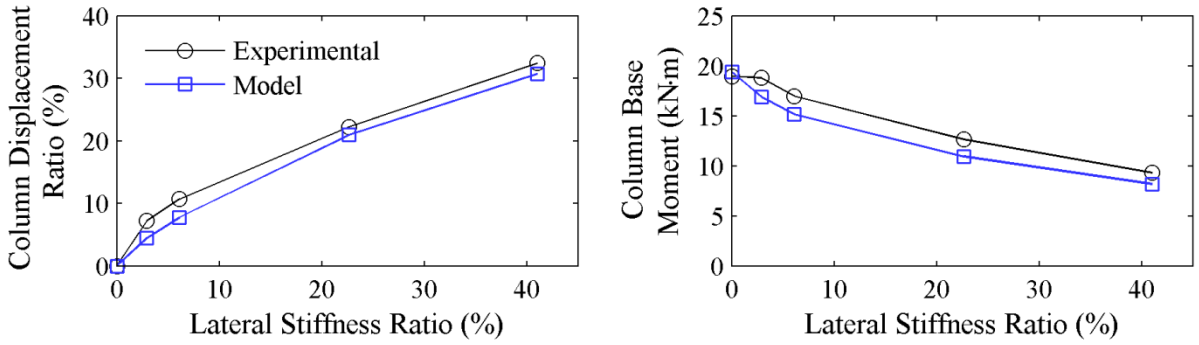

Fig. 12 – Effect of stiffness ratio on the column displacement ratio and base moment

also resulted in underestimating the peak base moment. Peak results were obtained at the end of the +/- 80 mm cycles to make relevant comparisons due to the HSS64x64x4.8 subassembly test being stopped early. The stiffness ratio of zero used the test results obtained from testing of the bearing without a column, simulating the bearing behavior when subjected to rigid boundary conditions. The column base moment at this stiffness ratio was obtained using the peak base moment of a rigid column subjected to the reactions measured at the bearing end plate from the bearing only test.

5. Conclusions

Seismic rehabilitation of at-risk structures using seismic isolation can provide excellent structural performance during earthquakes, but retrofit procedures tend to be expensive and limit applications to historical structures or buildings that require immediate occupancy following an earthquake. In order to reduce costs and extend the applications of isolation retrofit to a more general class of structures, isolation bearings may be placed on the tops of columns. This configuration mitigates many of the large contributors to project expenses for both retrofit and new construction; however, columns may not provide rigid boundary conditions to bearings causing end plates to not remain parallel. To investigate the effects of end plate flexibility on isolation bearings, and the column-bearing interaction in a column-top isolation system, experimental test of column-bearing subassemblies were conducted. Four subassemblies with varying column flexibilities were tested, and results are compared with an analytical bearing model able to capture the effects of end plate rotations. The key findings include

- End plate flexibility can significantly reduce the lateral stiffness of isolation bearings, and must be account for to accurately estimate the isolation bearing and peak displacement in the isolation layer.
- The analytical bearing model can represent the bearing behavior accurately at small rotations, but softening of the moment-rotation relationship, not characterized by the model, cause theoretical results to diverge from experimental at larger rotations.
- Experimental bending moment diagrams indicate columns act similar to fixed-free structures, and can be approximated as such when determining the lateral stiffness of supporting columns.
- Columns govern the rotation at the column-bearing interface due to a high rotational stiffness, and an expression derived using Euler-Bernoulli beam theory and assuming a fixed-free column provides accurate prediction of the rotations at the interface.

6. References

[1] Matsagar VA, Jangid RS (2008): Base isolation for seismic retrofitting of structures. *Practice Periodical on Structural Design and Construction*, 13 (4), 175-185.

[2] Naeim F, Kelly JM (1999): *Design of Seismic Isolated Structures: From Theory to Practice*. Wiley, New York.

[3] Tamura K, Nakamural Y, Saito T (2004): A new base-isolated long-span structure overhanging urban infrastructure. *Council on Tall Buildings and Urban Habitat*, Seoul, Korea.

[4] Pettinga D, Oliver S (2015): Aspects of the design for the base isolated Christchurch Justice and Emergency Services Precinct. *10th Pacific Conference on Earthquake Engineering*, Sydney, Australia.

[5] Post NM (2015): Seismic engineer develops 'showcase' for isolators. *Engineering News-Record*, August 24/31.

[6] Becker TC, Mahin SA (2013): Effect of support rotation on triple friction pendulum bearing behaviour. *Earthquake Engineering & Structural Dynamics*, 42 (12), 1731-1748.

[7] Mosqueda G, Whittaker AS, Fenves GL, Mahin SA (2004): Experimental and analytical studies of the friction pendulum system for the seismic protection of simple bridges. *Technical Report EERC 04-01*, Earthquake Engineering Research Center, Berkeley, USA.

[8] Karbakhsh Ravari A, Othman IB, Ibrahim ZB, Ab-Malek K (2012): P-Δ and end rotation effects on the influence of mechanical properties of elastomeric isolation bearings. *Journal of Structural Engineering*, 138 (6), 669-675.

[9] Rastgoo Moghadam S, Konstantinidis DA (2015): Effect of rotation on the horizontal behaviour of rubber isolators. *11th Canadian Conference on Earthquake Engineering*, Victoria, Canada.

[10] McKenna F, Fenves GL (2006): Open System for Earthquake Engineering Simulation (OpenSees). *Pacific Earthquake Engineering Research Center*.

[11] Haringx JA (1949): On highly compressible helical springs and rubber rods, and their application for vibration-free mountings, III. *Philips Research Reports 4*.

[12] Gent AN (1964): Elastic stability of rubber compression springs. *Journal of Mechanical Engineering Science*, 6 (4), 318-326.

[13] Imbimbo M, Kelly JM (1997): Stability aspects of elastomeric isolators. *Earthquake Spectra*, 13 (3), 431-449.

[14] Chang C (2002): Modelling of laminated rubber bearings using an analytical stiffness matrix. *International Journal of Solids and Structures*, 39 (24), 6055-6078.

[15] Crowder AP, Becker TC. Experimental investigation of elastomeric isolation bearings with flexible supporting columns. (Submitted: *Journal of Structural Engineering*, April 2016).

[16] Kelly JM, Konstantinidis DA (2011). *Mechanics of Rubber Bearings for Seismic and Vibration Isolation*. Wiley, New York.